Journal of Power Sources 195 (2010) 919–922

Contents lists available at ScienceDirect

Journal of Power Sources

journal homepage: www.elsevier.com/locate/jpowsour

Short communication

Pseudocapacitance of MnO_2 originates from reversible insertion/desertion of thiocyanate anions studied using in situ X-ray absorption spectroscopy in ionic liquid electrolyte

Ming-Tsung Lee [a], Wen-Ta Tsai [a], Ming-Jay Deng [b], Hui-Fang Cheng [b], I-Wen Sun [b], Jeng-Kuei Chang [a,*]

[a] Department of Materials Science and Engineering, National Cheng Kung University, 1 University Road, Tainan, Taiwan
[b] Department of Chemistry, National Cheng Kung University, 1 University Road, Tainan, Taiwan

ARTICLE INFO

Article history:
Received 12 June 2009
Received in revised form 18 August 2009
Accepted 19 August 2009
Available online 25 August 2009

Keywords:
Ionic liquid electrolyte
In situ X-ray adsorption spectroscopy (XAS)
Mn oxide
Energy storage
Insertion/desertion
Pseudocapacitance

ABSTRACT

Charge storage mechanisms of electrodeposited MnO_2 in various aprotic ionic liquids (ILs) are studied using in situ X-ray absorption spectroscopy (XAS). The analytical results show that a unique thiocyanate (SCN^-) anion can reversibly insert/desert into/from the tunnels between the [MnO_6] octahedral subunits depending on the applied potential. This process charge compensates the Mn^{3+}/Mn^{4+} redox transition upon charging–discharging and thus contributes to an ideal pseudocapacitive behavior of the MnO_2 electrode. The present work would open up a route for developing a novel oxide-based supercapacitor, with high cell-voltage, high thermal stability, and high safety, incorporating IL electrolytes.

1. Introduction

Development of alternative energy conversion/storage systems that can meet present day power demands has accelerated because of the environment issues and the depletion of fossil fuels. Supercapacitors, classified to double-layer capacitors and pseudocapacitors [1], are energy-storage devices that concurrently have a high power density, a large energy density, and a long cycle life; therefore, they have attracted much attention in wide applications. Pseudocapacitors, which involve bulk redox reactions of electrode materials and injections of protons or alkali cations in aqueous electrolytes [2–4], have a higher specific capacitance than double-layer capacitors. RuO_2 and a much cheaper alternative, MnO_2 [5–8], are typical oxide electrodes for pseudocapacitors.

ILs could be promising electrolytes for supercapacitors [9]. Owing to their wide potential windows, a large cell-voltage can be achieved which benefits both the energy density and power density of a supercapacitor. The non-volatility and non-flammability properties of ILs could eliminate the health and safety hazards rendered from organic solvent electrolytes. Moreover, the great thermal stability of ILs would enable a capacitor to reliably operate at elevated temperature. Although double-layer capacitors containing ILs have been extensively studied, using this kind of electrolyte in oxide-based pseudocapacitors remain challenges and is rarely investigated [10,11].

The critical point for showing pseudocapacitance in ILs is whether the constituent ions can become incorporated into the electrode, causing oxide to proceed a redox reaction. Rochefort and Pont suggested that a faradic transition of RuO_2 can only be performed in protic (proton-containing) 2-methylpyridine–trifluoroacetic acid (P–TFA) IL, but not in aprotic IL (without proton) [10]. However, this protic IL is not compatible with MnO_2 due to a serious corrosion problem [11]. The protons also limit the cathodic potential boundary of the IL where the hydrogen evolution occurs. In this communication, we demonstrate that by appropriately selecting the constituent ions of ILs an ideal pseudocapacitive performance of MnO_2 can be obtained in an aprotic electrolyte. In situ XAS studies help to elucidate the interaction mechanisms between MnO_2 and various ILs.

2. Experimental section

Mn oxide (0.3 mg cm^{-2}, with a thickness of about 1 μm) was electrodeposited on a Ni substrate from 0.25 M $Mn(CH_3COO)_2$ aqueous solution by applying an anodic potential of 0.8 V to give a total passed charge of 0.4 C cm^{-2} [12,13]. A platinum sheet and a saturated calomel electrode (SCE) were assembled as the counter

* Corresponding author. Tel.: +886 6 2757575x62942; fax: +886 6 2754395.
E-mail address: catalyst@mail.mse.ncku.edu.tw (J.-K. Chang).

0378-7753/$ – see front matter © 2009 Elsevier B.V. All rights reserved.
doi:10.1016/j.jpowsour.2009.08.047

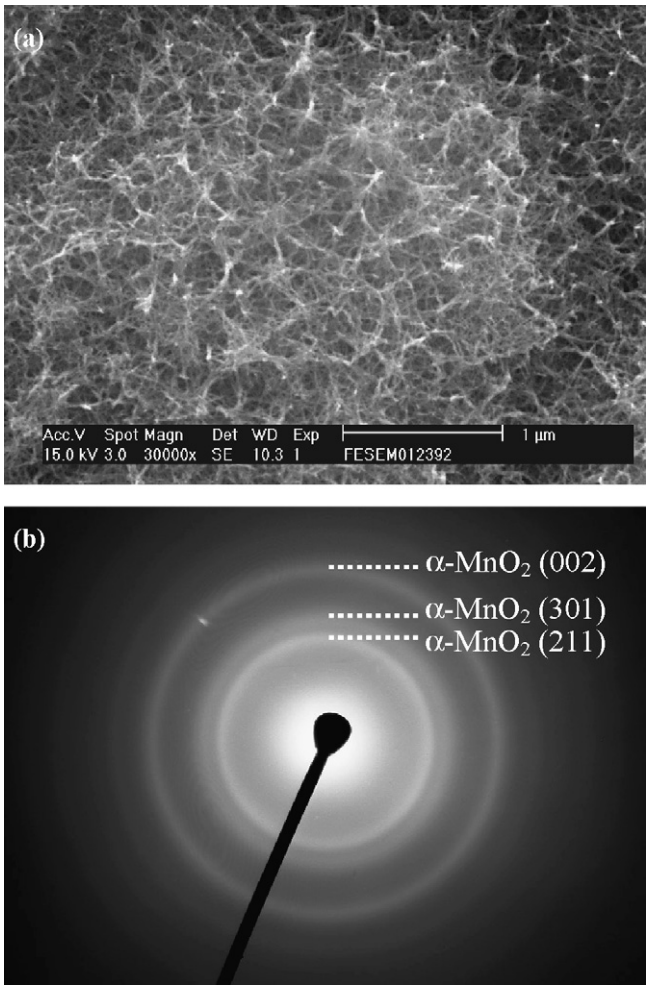

Fig. 1. (a) Surface morphology, examined using SEM, of the Mn oxide electrode prepared by anodic deposition. (b) Electron diffraction pattern of the Mn oxide examined with a TEM.

electrode and reference electrode, respectively. The surface morphology of the electrode was examined using a scanning electron microscope (SEM, Philip XL-40 FEG). A transmission electron microscope (TEM, JEOL 3010) was used to take the electron diffraction pattern (with a camera length of 120 cm).

The electrochemical properties of Mn oxide electrodes in ILs were studied using an AUTOLAB potentiostat at 25 °C in a nitrogen-purified glove box (Vacuum Atmospheres Co.), where both the moisture and oxygen contents were maintained below 1 ppm. The reference electrode was a Pt wire placed in a fritted glass tube containing butylmethylpyrrolidinium–bis(trifluoromethylsulfony)imide IL that had a ferrocene/ferrocenium couple (Fc/Fc^+ = 50/50 mol%, showing a potential of +0.55 V vs. SHE). The counter electrode was a spiral Pt wire, which was directly immersed in the bulk electrolyte.

In situ XAS studies under a fluorescence mode were performed at beam line 17 C of the National Synchrotron Radiation Research Center in Taiwan. The setup of the spectro-electrochemical cell and the detailed experimental conditions can be found in our previous paper [4].

3. Results and discussion

The SEM micrograph in Fig. 1(a) indicates that the electrodeposited oxide is composed of numerous interweaving nanowhiskers. The crystal structure of the oxide was analyzed using an electron diffraction technique; Fig. 1(b) shows the three major diffraction signals characteristic of the (2 1 1), (3 0 1), and (0 0 2) crystal planes of α-MnO_2 (JCPDS 44-0141). However, the faint diffraction rings suggest that the electrodeposited oxide is nanocrystalline and/or non-stoichiometric in nature.

Fig. 2(a) shows the cyclic voltammogram (CV) of an inert glassy carbon electrode recorded in 1-ethyl-3-methylimidazolium–thiocyanate (EMI–SCN) IL. The wide potential stability window (~2.4 V) indicates that this IL is a promising electrolyte for high cell-voltage supercapacitors. Fig. 2(b) exhibits the acquired CV curve of the MnO_2 electrode. The quasi-rectangular shape and mirror-image (in anodic and cathodic areas) feature, which show a capacitor-like response, can be recognized in a potential range stretching from −1.8 V to −0.3 V before irreversible cathodic and anodic reactions of the electrode took place. The much higher current density of Fig. 2(b) (as compared to Fig. 2(a)) implies that a redox reaction of MnO_2 may occur. Fig. 2(c) shows the chronopotentiogram (CP) of 10 sequent charge–discharge cycles of the MnO_2 electrode measured in EMI–SCN IL. Besides the ideal capacitive behavior, the high reversibility and great cyclic stability of the electrode were exhibited within a range of 1.5 V, which is larger than that (~1 V) typically found in traditional aqueous electrolytes [14,15]. From the CP data, the oxide specific capacitance is evaluated according to the following equation:

$$C = I/(\Delta E/\Delta t)w \quad (1)$$

where I is the applied current (0.1 mA), ΔE is the potential range (1.5 V × 2), Δt is the total charge–discharge time, and w is the mass of the oxide. The calculated specific capacitance of MnO_2 is 55 F g^{-1}. While the literature reported that RuO_2 showed an optimum capacitance of ~40 F g^{-1} in protic P–TFA IL [16], this study indicates that MnO_2, a much cheaper alternative, has an even better performance in aprotic EMI–SCN IL electrolyte. We also measured the specific capacitance of MnO_2 in other aprotic ILs, such as 1-ethyl-3-methylimidazolium–tetrafluoroborate (EMI–BF_4), 1-ethyl-3-methylimidazolium–bis(trifluoromethylsulfony)imide (EMI–nTf_2), and 1-butyl-3-methylimidazolium–hexafluorophosphate (BMI–PF_6). However, the capacitance values obtained were only around 20 F g^{-1}. Accordingly, the charge storage mechanism of MnO_2 in the different ILs was studied using in situ XAS.

Fig. 3(a) shows the Mn K-edge XANES (X-ray absorption near edge structure) spectra of the MnO_2 electrode measured under five different applied potentials in the sequence: −1.8 V, −1.05 V, −0.3 V, then back to −1.05 V, and finally −1.8 V in EMI–SCN IL. Although all the spectra do not exhibit considerable difference in shape, revealing a similarity in the structural characteristics of MnO_2 under various potentials, a clear energy shift of the adsorption peak, toward higher energy with increasing applied potential and returned to the initial position as the potential was switched back, can be recognized. This so-called chemical shift is related to the increase in binding energy of the core-level electron with increasing oxidation state [17]. Literature reported that the valent state of Mn can be identified by the absorption threshold energy (E_0), which can be obtained from the first inflection point on the absorption edge [18,19]. The E_0 values of MnO, Mn_2O_3, and MnO_2 reference samples were measured and shown in Fig. 3(b); an ideal linear relationship ($R^2 > 0.99$) between E_0 and the Mn oxidation state was found. According to the E_0 derived from the spectra in Fig. 3(a), the average Mn valance was determined to be 3.25, 3.45, 3.70, 3.50, and 3.27 in the sequence, as shown in Fig. 3(b). The results clearly confirm that a continuous and reversible faradic redox transition of MnO_2 indeed occurred in aprotic EMI–SCN IL, contributing the large capacitance found in Fig. 2. However, in the absence of protons and alkali cations in the electrolyte, what is

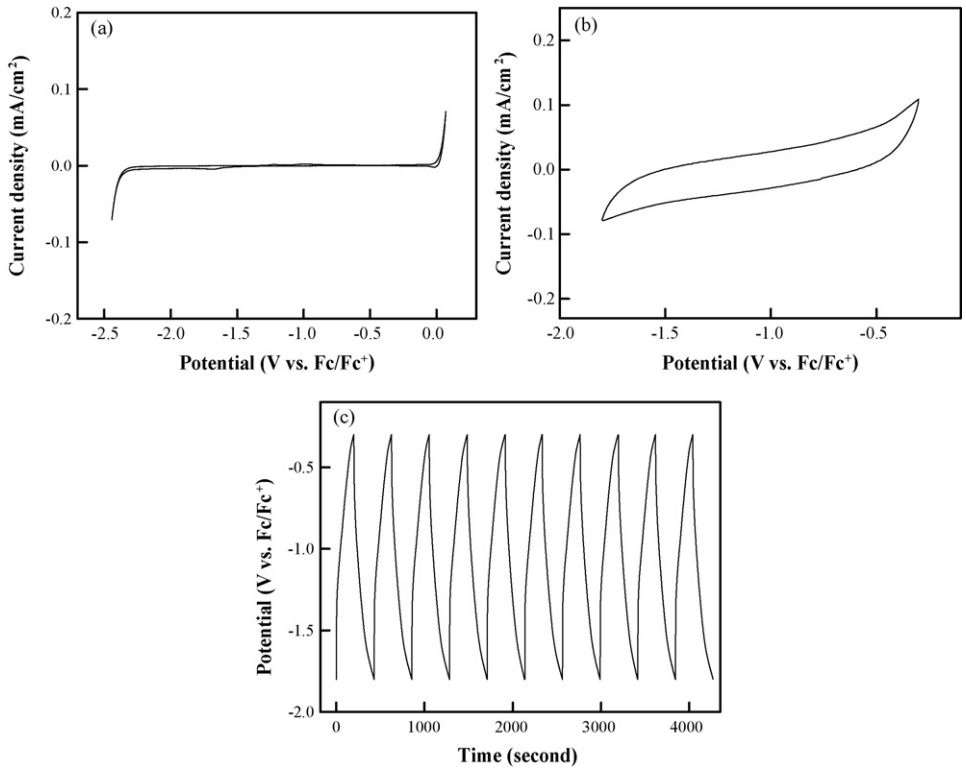

Fig. 2. Cyclic voltammograms of (a) an inert glassy carbon electrode and (b) the MnO_2 electrode recorded in EMI–SCN IL at a potential sweep rate of 3 mV s^{-1}. (c) Chronopotentiogram for 10 charge–discharge cycles of the MnO_2 electrode measured at an applied current density of ±0.1 mA cm^{-2}.

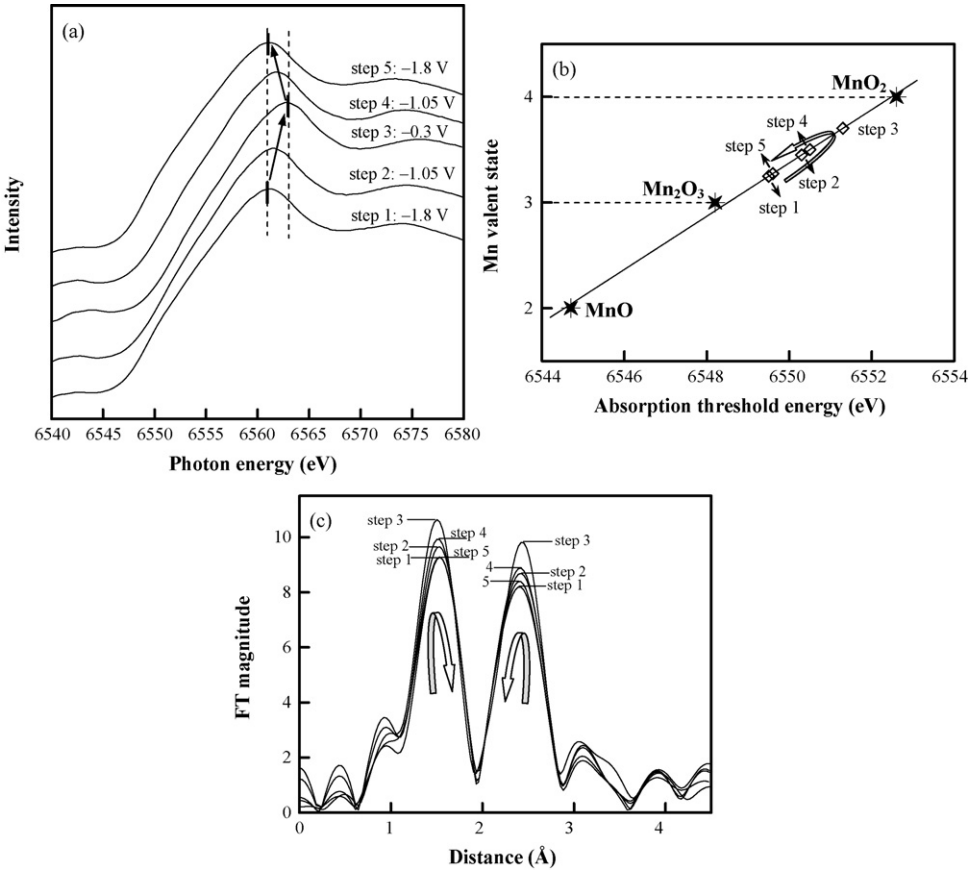

Fig. 3. (a) In situ Mn K-edge XANES spectra of the MnO_2 electrode. (b) The variation of the Mn valent state with respect with the applied potential. (c) In situ Mn K-edge EXAFS spectra of the MnO_2 electrode. The potentials were applied in the sequence: −1.8 V (step 1), −1.05 V (step 2), −0.3 V (step 3), then back to −1.05 V (step 4), and finally −1.8 V (step 5) in EMI–SCN IL.

the pseudocapacitive reaction mechanism? This issue was further clarified.

Fig. 3(c) shows the Fourier transformed (FT) magnitude of Mn K-edge EXAFS (Extended X-ray Absorption Fine Structure) spectra of the oxide electrode measured at the five sequent potentials in EMI–SCN IL. The first peak in the spectra around 1.5 Å is attributed to an interaction with oxygen in the first coordination shell (i.e. Mn–O bond within a [MnO_6] octahedral unit, which builds the structural framework of MnO_2). The shift of the Mn–O peak, toward a lower interatomic distance at a higher applied potential, was associated with an oxidation reaction since the ionic radius of Mn^{4+} (0.53 Å) is smaller than that of Mn^{3+} (0.64 Å) [20]. The second peak located near 2.5 Å corresponds to the nearest Mn atoms in the second coordination shell (i.e. Mn–Mn bond between the neighboring [MnO_6] units). As shown, increasing the potential led to a clear increase of the Mn–Mn bond length, indicating the expansion between the [MnO_6] octahedral units. The opposite shift directions of the two peaks in the figure indicate that the linear-shape SCN^-, rather than the larger EMI^+ with an imidazolium ring, is the primary working ion that can insert into the tunnel between the [MnO_6] units and charge compensates the Mn valent state variation. Moreover, a reversibility of the insertion/desertion reaction upon charging/discharging is clearly recognized in Fig. 3(c) (i.e. reducing the electrode from −0.3 V back to −1.8 V resulted in the EXAFS spectrum returning to its original state). Accordingly, a pseudocapacitive mechanism of MnO_2, based on the working of SCN^- anions in the IL electrolyte, can be proposed as follows:

$$MnO_{2-x}(SCN)_{2x} + 2xe^- \leftrightarrow MnO_{2-x} + 2xSCN^-(x \leq 0.5) \quad (2)$$

It was noted that, in the other three aprotic ILs, neither the Mn oxidation state variation nor the Mn–Mn bond length charge can be found. Accordingly, the participation of EMI^+ in Eq. (2) can be excluded. The data also revealed that the BF_4^-, PF_6^-, and nTf_2^- anions cannot insert into MnO_2, probably due to the size and geometry limitations. Benedetti et al. suggested that, according to their EQCM data, nTf_2^- could electroneutralize the MnO_2 film at the superficial sites [21], our present study confirms that this anion cannot insert into MnO_2 and thus hardly causes a bulk redox reaction. Since only surface double-layer capacitance, instead of pseudocapacitance, was involved, the measured capacitances in these three electrolytes were much lower, as described above.

4. Conclusion

In summary, it is possible for MnO_2 to perform ideal pseudocapacitive behavior in aprotic IL. The advantages of using IL electrolyte in a supercapacitor as least include allowing high-temperature applications and high cell-voltage, and minimize the safety and environmental hazards. In situ XAS analyses suggested that the unique SCN^- anions could reversibly insert/desert into/from the tunnels between the [MnO_6] units and charge compensate the Mn^{3+}/Mn^{4+} redox transition during charging/discharging, thus contributing to the pseudocapacitance. Designing more suitable constituent ions in IL electrolytes (with proper physicochemical characteristics and desired interaction with various oxides) is already in progress, in order to further improve the electrochemical performance of supercapacitors and other charge storage devices.

Acknowledgement

The financial support of this work, by the National Science Council of the Republic of China under Contract No. 98-ET-E-006-009-ET, is gratefully acknowledged.

References

[1] B.E. Conway, Electrochemical Supercapacitors, Kluwer-Plenum, New York, 1999.
[2] C.C. Hu, T.W. Tsou, Electrochem. Commun. 4 (2002) 105–109.
[3] M. Toupin, T. Brousse, D. Bélanger, Chem. Mater. 16 (2004) 3184–3190.
[4] J.K. Chang, M.T. Lee, W.T. Tsai, J. Power Sources 166 (2007) 590–594.
[5] A.E. Fischer, K.A. Pettigrew, D.R. Rolison, R.M. Stroud, J.W. Long, Nano Lett. 7 (2007) 281–286.
[6] R. Liu, S.B. Lee, J. Am. Chem. Soc. 130 (2008) 2942–2943.
[7] C.C. Hu, Y.T. Wu, K.H. Chang, Chem. Mater. 20 (2008) 2890–2894.
[8] J.K. Chang, C.H. Huang, W.T. Tsai, M.J. Deng, I.W. Sun, J. Power Sources 179 (2008) 435–440.
[9] H. Ohno, Electrochemical Aspects of Ionic Liquids, John Wiley & Sons., Hoboken, 2008.
[10] D. Rochefort, A.L. Pont, Electrochem. Commun. 8 (2006) 1539–1543.
[11] J.K. Chang, M.T. Lee, C.W. Cheng, W.T. Tsai, M.J. Deng, I.W. Sun, Electrochem. Solid-State Lett. 12 (2009) A19–A22.
[12] J.K. Chang, W.T. Tsai, J. Electrochem. Soc. 150 (2003) A1333–A1338.
[13] J.K. Chang, Y.L. Chen, W.T. Tsai, J. Power Sources 135 (2004) 344–353.
[14] H.Y. Lee, J.B. Goodenough, J. Solid State Chem. 144 (1999) 220–223.
[15] S.C. Pang, M.A. Anderson, T.W. Chapman, J. Electrochem. Soc. 147 (2000) 444–450.
[16] L. Mayrand-Provencher, D. Rochefort, J. Phys. Chem. C 113 (2009) 1632–1639.
[17] M. Belli, A. Scafati, A. Bianconi, S. Mobilio, L. Palladino, A. Reale, E. Burattini, Solid State Commun. 35 (1980) 355–361.
[18] P. Ghigna, G. Flor, G. Spinolo, J. Solid State Chem. 149 (2000) 252–255.
[19] F. Farges, Phys. Rev. B 71 (2005) 155109.
[20] R.D. Shannon, Acta Crystallogr. 32 (1976) 751–767.
[21] T.M. Benedetti, F.F.C. Bazito, E.A. Ponzio, R.M. Torresi, Langmuir 24 (2008) 3602–3610.